Journal of Applied Fluid Mechanics, Vol. 13, No. 1, pp. 103-117, 2020.
Available online at www.jafmonline.net, ISSN 1735-3572, EISSN 1735-3645.
DOI: 10.29252/jafm.13.01.29970

Experiments and Large-Eddy Simulations of Lobed and Swirling Turbulent Thermal Jets for HVAC's Applications

A. Bennia[1,2†], H. Fellouah[3], A. Khelil[1], L. Loukarfi[1] and H. Naji[4]

[1] *Department of Electromechanics, Mohamed El Bachir El Ibrahimi University, Bordj Bou Arreridj, El-Anasser, 34030, Algeria*
[2] *Control, Testing, Measurement and Mechanical Simulation laboratory, University Hassiba Benbouali of Chlef, Hay Salem, National Road N° 19, 02000, Algeria*
[3] *Department of Mechanical Engineering, University of Sherbrooke, 2500 University Boulevard, Sherbrooke, Quebec, Canada.*
[4] *University of Artois, University of Lille, IMT Douai & Yncréa Hauts de France/ LGCgE, LGCgE (Ea 4515), F-62400 Béthune, France*

†*Corresponding Authors Emails: Abderazak.Bennia@USherbrooke.ca*

(Received January 2, 2019; accepted May 27, 2019)

ABSTRACT

The mixing improvement by passive control is of wide practical interest. The lobed diffuser, which mixes the primary and secondary streams with high efficiency, has been widely used for heat and mass transfer in the field of fluid engineering. In addition, the jets through lobed generate streamwise vortices, which mix the ambient air and the jet fluid more effectively. The main objective of the present work is to develop new air diffusers for heating, ventilation, air conditioning (HVAC) systems using different jet geometries, in order to improve the users' thermal comfort. Three free jets of air diffusers emitted from a tubular lobed, with six and five lobes, and from a swirl nozzle have been both studied experimentally and numerically. All diffusers have the same throat diameter. It turns out that the results obtained with the LES/WALE and LES/K-ET turbulence models are respectively in good agreement with the experimental results of the lobed and swirling jets. These results indicate that the best mixture is obtained using the six-lobed nozzle with respect to the five-lobed nozzle and the swirling nozzle. In addition, the importance of the jet type on the mixing capacity is highlighted.

Keywords: Lobed jets; Swirling jet; Thermal homogenization; Experimental study; Numerical simulation; LES.

NOMENCLATURE

D_e	equivalent diameter
H	lobe height
L	lobe length
P	pressure in the jet cross-section
Re	Reynolds number
S	Swirl number
$T_{r_{exp}}$	experimental reduced temperature
$T_{r_{exp}}$	numerical reduced temperature
U_0	mean velocity at the diffuser exit
r/D_e	dimensionless radius (radial direction)
X/D_e	dimensionless height (axial direction) due to the mean velocity gradient
α_a	angles of the vanes with the jet axis
α_b	angles of the vanes with the plane of blow
θ_{ext}	exterior angle of the lobes
θ_{int}	interior angle of the lobes
μ	dynamic viscosity
ν	kinematic viscosity
ρ	fluid density

Acronyms

LES	Large-Eddy Simulation
LES/K-ET	Kinetic-Energy Transport model
LES/S-L	Smagorinsky-Lilly model
LES/WALE	Model Wall-Adapting Local Eddy Viscosity
MP	Major plane
mP	Minor plane

1. INTRODUCTION

Researches on the mixing physics and on the mechanisms to improve it are necessary for many engineering applications. Over the past few decades, it has become clear that the generation of vortices in a mixing flow using certain vortex generators such as lobed and/or swirling nozzles is an extremely powerful mechanism for improving flow mixing. To improve the diffusion efficiency at a lower cost by taking into account the aesthetic appearance of the units designed, a passive system blowing the jet through the lobed diffuser or the swirling nozzle is a good alternative. Their applications are very numerous. These include jet engine thrust, pollutant dispersion, air conditioning, ventilation and heating systems used in the building (Dimotakis 2000). These geometries showed till now their efficiency in the aeronautic and aero spatial domains (Nastase *et al.*, 2011). Also, the diffusers lobed used in the injectors design and in the domain of combustion offering good combustion stability (Meslem *et al.*, 2010; Elhassan *et al.*, 2011; Nastase *et al.*, 2011). The mixing improvement by passive control is of wide practical interest. This passive control allows the improvement diffusion of air in the habitation. (Meslem *et al.*, 2012). The objective of the works done in LEPTIAB (University of la Rochelle, *France*) since 2003 on the jets, is to transpose the asymmetric diffuser idea of the aeronautics fields, aero spatial and the combustion domains to that of the air diffusion of building (Nastase, 2007; Meslem *et al.*, 2008; Nastase *et al.*, 2010; Elhassan *et al.*, 2010; Meslem *et al.*, 2011). A lobed nozzle has circular cross-section at the inlet and a convoluted shape at the exit. It generates strong streamwise vortices at the nozzle exit itself thereby enhancing the near-field mixing. The vortex enhanced mixing has become one of the highly targeted research areas in recent years (Depuru *et al.*, 2015). Many investigations are carried out to improve the air mixture, like the works published by Tilman *et al.* (1993); Presz *et al.* (1994); Power *et al* (1994); Hu *et al.* (1996) and Smith *et al.* (1997) to name a few. Paterson *et al.* (1982) have been among the first to measure the turbulent characteristics and velocity of a lobed diffuser. Likewise, Ukeiley *et al.* (1993, 1992) and Glauser *et al.* (1996) have hydrodynamically characterized the flow jet of a lobe mixer. Some works (Oyakawa *et al.*, 1998) have been conducted to study the convection coefficient of impinging lobed jets. The use of rectangular tabbed or circular diffusers has demonstrated their mixing performance efficiency over circular and rectangular diffusers without tabs. (Zaman 1996a, b; Hu *et al.*, 1999, 2000). Each tab generates a pair of counter-rotating streamwise vortices that modify up the turbulent structures of the jet flow, thus increasing the performance of its mixing with the secondary flow. Diffusers geometry has also been oriented towards more complex shapes (Belovich *et al.*, 1997; Yuan, 2000), and recent works (Hu *et al.*, 2001; Zaman *et al.*, 2003) that the lobed diffuser is a good mixing device. The effect of a number of lobes on aerothermodynamic performance of lobed S-shaped two-dimensional nozzle was investigated by Li-wei (2015). Their results show that the degree of mixing is highly affected by the number of lobes and the thermal mixing efficiency increases with the lobes number. Bennia *et al.* (2015) conducted an experimental investigation on a lobed jet diffuser, applied to comfort in residential premises. The objective was the optimization of air diffusion by the application of lobed diffuser jets. The axial temperature of jet measurements, up to 20 De, for the diffuser with lobes, at a low height and at wider opening, and for the diffuser without and with swirling, show that in the same blowing conditions, the jet of lobed provides better temperature stability in the radial direction while the swirling jet, at an inclination angle of 60°, ensures a better expansion of the radial temperatures. In a recent study, Bennia *et al.* (2016; 2018) also interested in improving air diffusion in the building by using diffusers with lobes. The numerical results obtained with the RNG k-ε and SST k-ω models are found in good agreement with the results of experimental. The obtained results show the interest of the characteristics of this type of jet for its application to the residential HVAC systems.

Swirling jets are often used to improve thermal transfer in HVAC systems. The azimuthally motion can be generated by different mechanisms such as tilted vanes. Understanding of swirl effects is very important for the ventilation system efficiency. Studies on swirling jets indicated that the swirl jet would develop more rapidly than circular jet. Near the blowing origin, the profiles are characterized by irregularities due to the swirling geometry (Palsson *et al.*, 2013). Recent researches on swirling jets have shown that these spread a great deal and induce a good mix of jets without swirling (Khelil *et al.*, 2009; Ranga *et al.*, 2010). Moreover, it has been reported that the vortex leads to both a rapid spread and a mixture of the jet. Also, it seems that at the orifice origin, the velocity profiles are typified by no-uniformity due to both the swirler's complex geometry and blowing conditions (Choi *et al.*, 2012; Lee, 2008; Braikia *et al.*, 2012).

The main objective of this study is to establish the temperatures distribution for two jets configurations from a lobed nozzle and one configuration from a swirling nozzle, using «ANSYS-CFD (v.16.1)». These types of flows have been studied with a view to their application to ventilation in residences.

2. EXPERIMENTAL METHODOLOGY

The experimental setup has been specifically designed to generate an air jet by lobed and swirling diffusers. The experimental room is 2.5 m wide, 2.5 m high and 3.0 m long (Fig. 1). Note that, during the experiments, the room was isolated from the outside environment, and due to the lack of thermal control at the room walls, the ambient temperature was not kept constant.

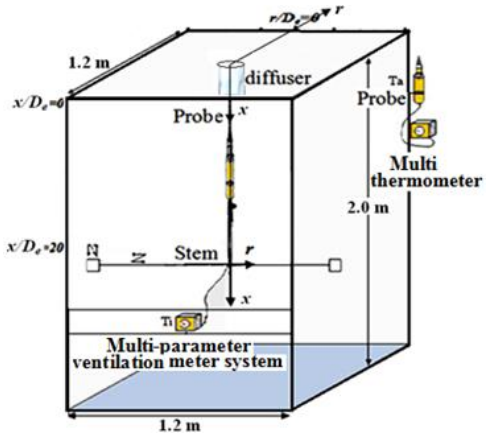

Fig. 1. Schematic description of the experimental setup.

The difference in temperature between the environment and the jet is monitored by readjustment of the air temperature by blowing. Thereby, the number of Archimedes remains constant during the experiments. The setup consists of a blowing device attached to the chassis frame. The latter includes an air diffuser directed from top to bottom. The temperatures and velocities of flow have been measured by a multi-parameter ventilation meter system. To scan the maximum space, we use a stem supporting a probe guided horizontally and vertically. Outside the flow, we placed a multi-thermometer to measure the instantaneous ambient temperature (T_a). The ambient temperature T_a and the jet temperature T_i, at different points, are measured simultaneously. The two temperatures were not taken until they were stable. The reduced temperature ($T_r = \frac{T_i - T_a}{T_{max} - T_a}$) is calculated with respect to the difference between the mean maximum temperature at the blowing opening and the ambient temperature (Suleiman *et al.*, 2004).

The measuring devices used in our study are presented in Table 1 below.

Table 1 Experimental measuring devices

Measuring device	Model
Multi-parameter ventilation meter system	TSI VELOCICALC PLUS 8386-M-GB (accuracy of ±3% of the reading)
Multi-thermometer	General Tools DKP300MA Digital Alarm Thermometer Waterproof (accuracy of ±0.1°C)

Figure 2 depicts the lobed diffuser with six lobes and six troughs. The angle of inclination of the troughs is 22 ° inwards. The diffuser is a length of 0.09 m and a diameter of 0.052 m. The lobe has a wider opening, a height of 0.012 m and a width of 0.008 m.

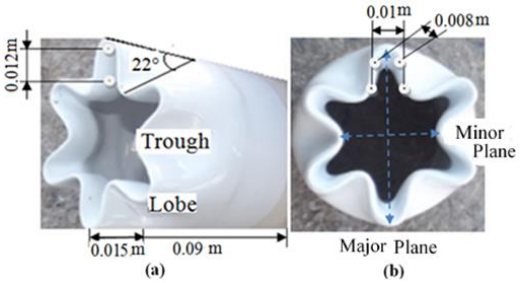

Fig. 2. (a) Photography of a lobed nozzle with 6 lobes, (b) Geometry of the blowing plane (yz).

Figure 3 shows the five-lobed five-trough lobe diffuser. The angle of inclination of the hollows is 22 ° inwards. The diffuser has a length of 0.09 m and a diameter of 0.052 m. Its height is 0.015 m and its width is 0.001 m.

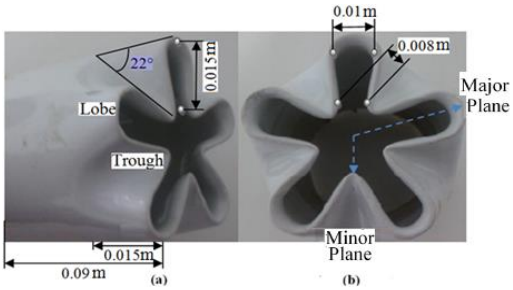

Fig. 3. (a) Photography of a lobed nozzle with 5 lobes, (b) Geometry of the blowing plane (yz).

Figure 4 shows a swirl nozzle with eleven aluminum vanes arranged on an aluminum holder of a diameter d of 0.022 m. To achieve a vortex effect, the vanes are oriented at inclination angles α_a of 30° and α_b of 60° with respect to the jet axis and the plane of blow, respectively. The vanes are arranged to be connected to a fixed support (vane support) behind which develops a recirculation zone whose length depends on the blowing device having a diameter D_e which refers to the diameter of the blow origin.

To perform the experiments, the conditions of the following operations have been taken into account: the Reynolds number (Re=3.0*10^5), volumetric flow rate (Q_v=0.019 m^3.s^{-1}), velocity inlet (U=7.7 m.s^{-1}), air $_{initial}$ temperature at the blowing orifice (T=323.3 K), radial direction (r/D_e=1 to 4) and axial direction ($0 \leq x/D_e \leq 20$). It should be noted that for the three air jets, our study was based on the same Reynolds number and volumetric flow rate. For the swirl nozzle, the swirling number used in our investigation is S=1.3.

3. Experimental Results And Discussion

3.1 Experimental Comparison of Axial and Radial Temperature Profiles

The assessment of the relevance of the integration of jet diffusers in the field of air ventilation in residential areas and transport zones requires a

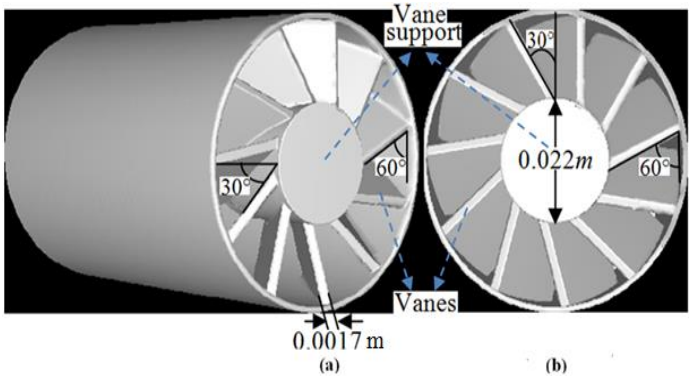

Fig. 4. (a) Photography of a swirling nozzle, (b) Geometry of the blowing plane (YZ).

comparative study of a swirling jet with two lobed jets under adequate blowing conditions.

- **Axial Temperature Profiles**

Figure 5 shows the axial distribution of the reduced temperature obtained with the six- and five-lobed jets and the swirling jet under the same conditions. Note that the three nozzles have the same equivalent diameter and operating conditions.

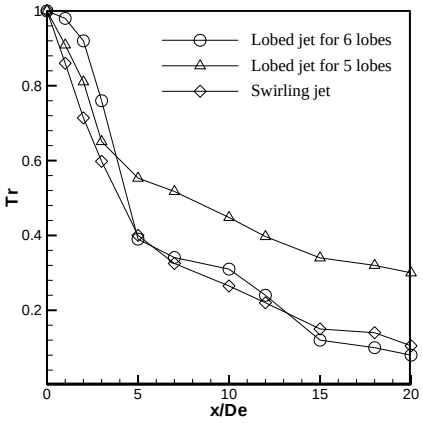

Fig. 5. Comparison of axial temperature profiles for two lobed jets and the swirling jet in free mode.

The induction generated by each jet causes a rapid decrease in temperature in the axial direction which stabilizes away from the blowing pore for the three jets. It is of the order of 38% (for the six-lobed jet), 50% (for the five-lobed jet) and 40% (for the swirling jet) of its initial value and this, over a distance of $5D_e$ from the blowing axis. From $5D_e$ to $15D_e$, a second slope, much less accentuated, was observed. Beyond 15 D_e, the heat intensity stabilizes and regulates along the flow for the three jets.The rapid decrease results in a transfer of energy to the radial direction. As a result, the jet eventually "dilutes" in the ambient fluid and its initial energy is dissipated because it is in a fully turbulent flow with vortices with various sizes. These are anisotropic (they deform in the mean flow direction) and contain most of the energy. These large eddies transmit their energy sequentially to smaller vortices (without loss of energy).This process continues until the energy is fully transmitted to small vortices where a viscous energy dissipation occurs. It is worth noting here that, prior to reaching these smaller vortices, viscosity plays no role. The decrease in axial temperature (see Fig. 5) allowed estimating the lengths of the potential nuclei for the swirling jet, the 5-lobed jet and the 6-lobed jet at $5D_e$, $3D_e$ and $1D_e$, respectively. The rapid decrease in the axial temperature of the 6-lobed jet explains the energy transfer in the radial direction. This is the purpose of the next section for radial temperature profiles. Furthermore, the results obtained through the lobe diffusers allow quantifying the relative importance of the lobes number and the troughs inclination with respect to the blowing plane. Moreover, a lower turbulent kinetic energy developed far from the blow (particularly in the turbulent region) could lead to low energy dissipation, which could, however, have a greater range. In addition, the result obtained by the swirling jet determines the importance of vanes tilt and its impact on the creation of the swirling flow outside the diffuser. On the basis of the work of Braikia *et al.* (2012) on the swirling jet, the tilt angle $\alpha = 60°$ is retained here. These authors have shown that with a tilt angle $\alpha = 60°$, a more rapid decrease of the temperature is obtained, which generates a greater thermal spread with respect to the other tilt angles, namely $\alpha = 0°$ and $\alpha = 30°$.

This finding also highlighted the importance of this type of jets in the heating, ventilation and air conditioning (HVAC) field, because of their low cost, their aesthetic and their efficiency characteristics of mixing. In particular, the advantage of the 6-lobed jet over the 5-lobed jet and the swirling jet with a 60 ° inclination is clearly shown.

- **Radial Temperature Profiles**

The analysis of radial temperature profiles highlights the importance and role of jet type in the air flow mixing performance. Figure 6 shows the radial temperature distribution for the three jets. In similar blowing conditions, it shows that the lobed jets can better ensure the stability of radial temperatures, while the swirling jet with an

inclination angle of 60° can better allow the expansion of radial temperatures. Concerning the six-lobed jet and the swirling jet, the temperature distribution in the same plane (*yy'*or *zz'*) is almost axisymmetric indicating an equal transfer capacity in same directions ([*-y, +y*] or [*-z, +z*]). In contrast, the five-lobed jet becomes almost axisymmetric in the fully developed region. For radial temperatures, the lobed jet with 6 lobes provides a relative regularity profiles and a expansion not negligible, thus, high thermal homogenization for a given position. Radially, temperature stabilization is of greater importance in the lobed jet with 6 lobes than in the lobed jet with 5 lobes and the swirling jet with an inclination angle of 60°.

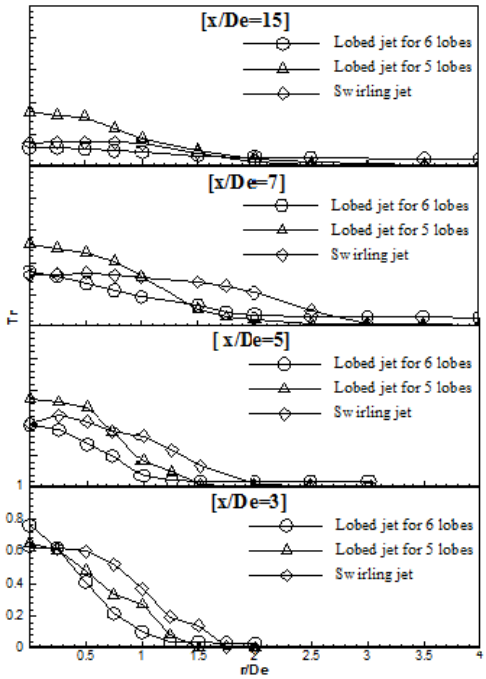

Fig. 6. Comparaion of the radial temperature profiles of two lobed jets and the swirling jet in free mode.

The lobe nozzles generate at the end of each lobe a pair of vortices with opposite directions of rotation. This improves the mixing capabilities of this type of nozzle versus a swirling nozzle. The influence of the lobed geometry on heat transfer depends on the number of lobes which have a major influence on the mechanisms of local heat. A nozzle having more lobes will generate more turbulence and improves the heat, thereby improving the thermal homogenization. The lobed geometry of the nozzle would thus be responsible for this "cutting" and the longitudinal structures are generated here by shearing of the transverse flow produced by the variation of the boundary radius of curvature of the nozzle and accentuated by the lobes and the inclination hollow. If one seeks to improve the mixing quality by minimizing the loss, the lobed nozzle with 6 lobes provides the best model. The radial temperature decrease is due to mixture effect of the environment with the jet and the possible loss of heat.

In this case, the six-lobe jet with flared opening and low height is more efficient than the others. As a result, it allows good mixing and a net homogenization atmosphere confirming the mixing performance of the expected six-lobed jet.

3.2 Experimental Radial Temperature Profiles of the Six-Lobed Jet

Figure 7 presents the radial profiles of temperature, in the major and minor planes, measured at different axial positions for the lobed jet with 6 lobes.

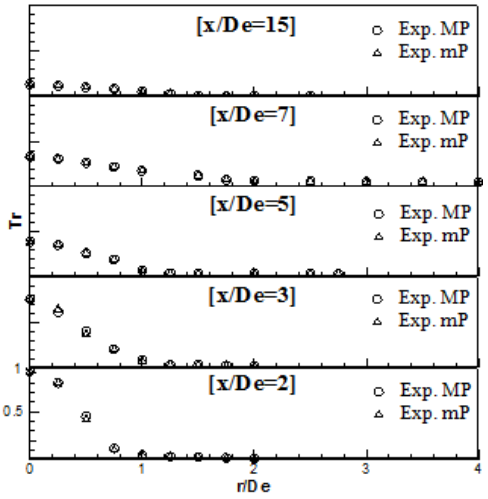

Fig. 7. Radial temperature profiles of the 6-lobed jet.

The recorded measurements (not shown here) obtained at x/D_e=1 for the entire jet showed that, in the same plane (major or minor), the jet is axisymmetric indicating equal heat transfer in all directions. In the plane of symmetry, the temperature reaches its maximum close the axis of jet, and then diminishes in the radial direction to stabilize when it moves away from the axis of jet, for the two planes. From the axial positions $1D_e$ to the $5D_e$, a clear influence of the major plane on the temperatures radial expansion is observed. A light decrease of temperature in the case of the minor plane is also observed. This difference can be explained by the more flared opening influence of lobes. From the axial position $5D_e$ up $20D_e$, the jet is not influenced by the lobes and the troughs. Since the jet looks like a circular jet, the temperature profiles are similar with the same expansion in the radial direction for both the major and minor planes.

3.3 Experimental Radial Temperature Profiles of the Five-Lobed Jet

Recorded measurements for the studied lobed jet configuration (with 5 lobes) have been performed for the entire radial position of jet; the negative values of r/D_e are for the major plane while the positive values of r/D_e are for the minor plane for. The result is shown in Fig. 8 for different axial positions. It is clear that, from the axial position $1D_e$ to $7D_e$, the major plane gifted a relative expansion radial of temperatures compared to the minor plan. Beyond the station $x=7D_e$, the radial spreading is

the same for the two planes (major and minor) which due to the fact that the lobed jet becomes circular.

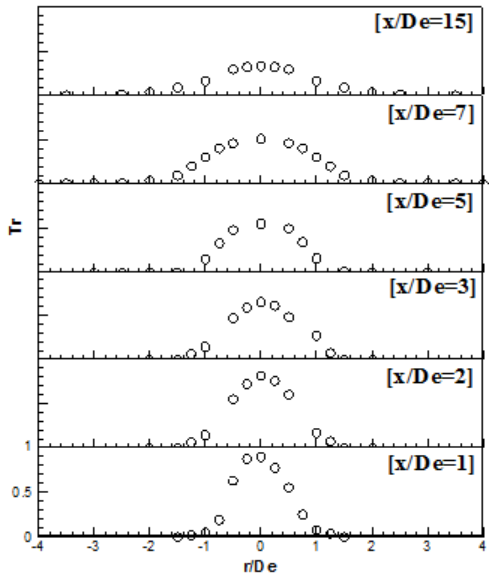

Fig. 8. Radial temperature profiles of the 5-lobed jet. Negative values of r/D_e are for the Major plane and positive values are for the minor plane.

3.4 Experimental Radial Temperature Profiles for the Swirling Jet

Figure 9 depicts the radial temperature profiles at different measurement positions in the case of swirling jet.

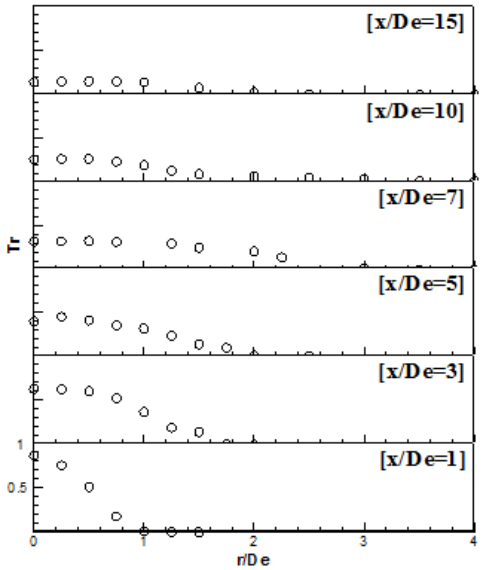

Fig. 9. Radial temperature profiles of the swirling jet.

It shows that, at the position x/D_e=5, the temperature increases until a maximum value close to r/D_e=0.25, and then it decreases rapidly to r/D_e=2, the point after which the temperature stabilizes with a pretty variation. The increase in temperature between r/D_e=0 and r/D_e=0.25 is due to the design of the air generator, the periphery of the blowing orifice being hotter than its center. This explains why the temperature in the center of the jet is quite low. For the positions x/D_e=7, 10 and 15, similar profiles to that of the station x/D_e=5 were obtained. This allows drawing an analogous interpretation with the exception that the maximum temperature is low and that the temperature increases to reach its maximum value close to r/D_e=0.5. Then it starts to decrease rapidly in the radial direction.

4. Numerical Simulations

Recall that Large eddy simulation is used in the present work. LES directly computes the large-scale turbulent structures, which are responsible for the transfer of energy and momentum in a flow, while modeling the smallest dissipative structures that are assumed to be isotropic. To distinguish large and small scales, a filter function is used to fix large eddies by introducing a length scale denoted Δ (filter cutoff width) which is a characteristic of the simulation considered (Jones *et al.*, 2008). In other words, all eddies with size larger than Δ are resolved directly, while those with size smaller than Δ are approximated.

4.1. Filtered Navier-Stokes equations

For incompressible Newtonian fluid, the equation of continuity and the equations of Navier-Stokes are filtered, yielding the filtered incompressible continuity equation (Leonard, 1974):

$$\frac{\partial \bar{u}_i}{\partial x_i} = 0 \tag{1}$$

and the filtered Navier-Stokes equations:

$$\frac{\partial \bar{u}_i}{\partial t} + \frac{\partial}{\partial x_j}\left(\bar{u}_i \bar{u}_j\right) = -\frac{1}{\rho}\frac{\partial \bar{p}}{\partial x_i} + 2\nu \frac{\partial}{\partial x_j}\left(\bar{S}_{ij}\right) - \frac{\partial \tau_{ij}^r}{\partial x_j} \tag{2}$$

with the residual stress tensor τ_{ij}^r grouping all unclosed terms. Leonard (1974) decomposed this tensor as $\tau_{ij}^r = L_{ij} + C_{ij} + R_{ij}$ and provided physical interpretations for each term. L_{ij} is the Leonard tensor that represents the interactions among large scales, R_{ij} is the Reynolds stress-like term that represents the interactions among the sub-filter scales (SFS), and C_{ij} is the Clark's tensor (Clark et *al.*, 1979) representing cross-interactions between large and small scales (Leonard ,1974).

Filtering the energy equation gives:

$$\frac{\partial \rho \bar{h}_s}{\partial t} + \frac{\partial \rho \bar{u}_i \bar{h}_s}{\partial x_i} - \frac{\partial \bar{p}}{\partial t} - \bar{u}_j \frac{\partial \bar{p}}{\partial x_i} - \frac{\partial}{\partial x_i}\left(\lambda \frac{\partial \bar{T}}{\partial x_i}\right) = -\frac{\partial}{\partial x_j}\left[\underbrace{\rho(\overline{u_i h_s} - \bar{u}_i \bar{h}_s}_{\text{Subgrid enthalpy flux}}\right] \tag{3}$$

where λ and h_s are the thermal conductivity and sensible enthalpy, respectively.

4.2. Subgrid-Scale Models

The subgrid-scale stresses resulting from filtering operations are unknown and require modeling. In ANSYS Fluent, the subgrid-scale turbulence models use the Boussinesq hypothesis (Clark *et al.*, 1979) as in the RANS models, computing subgrid-scale turbulent stresses from the following relationship:

$$\tau_{ij} - \frac{1}{3}\tau_{kk}\delta_{ij} = -2\mu_t \bar{S}_{ij} \tag{4}$$

where μ_t is the subgrid-scale turbulent viscosity. The isotropic part of the subgrid-scale stresses τ_{kk} is not modeled, but added to the filtered static pressure term. $\bar{S}_{ij}$ is the strain rate tensor for the resolved scale defined by:

$$\bar{S}_{ij} \equiv \frac{1}{2}\left(\frac{\partial \bar{u}_i}{\partial x_j} + \frac{\partial \bar{u}_j}{\partial x_i}\right) \tag{5}$$

$$\tau_{ij} - \frac{1}{3}\tau_{kk}\delta_{ij} = -2\mu_t\left(S_{ij} - \frac{1}{3}S_{kk}\delta_{ij}\right) \tag{6}$$

Note that for incompressible flows, the term involving τ_{kk} can be added to the filtered pressure or simply neglected (Erlebacher *et al.*, 1992).

- **Smagorinsky-Lilly Model**

This simple model was first proposed by Smagorinsky (1963). In the Smagorinsky-Lilly model, the eddy-viscosity is modeled by

$$\mu_t = \rho L_s^2 \left|\bar{S}\right| \tag{7}$$

where L_s is the mixing length for subgrid scales and $|\bar{S}| \equiv \sqrt{2\,\bar{S}_{ij}\bar{S}_{ij}}$. In ANSYS Fluent, L_s is computed as follows:

$$L_s = \min(\kappa d, C_s \Delta) \tag{8}$$

where κ is the von Kármán constant, d is the distance to the closest wall, C_s is the Smagorinsky constant, and Δ is the local grid scale. In ANSYS Fluent, Δ is computed according to the volume of the computational cell using.

$$\Delta = V^{1/3} \tag{9}$$

- **Dynamic Smagorinsky-Lilly Model**

In the dynamic model, the LES constant varies not only in space, but also in time. Therefore, two different filters are recommended (Germano *et al.*, 1996). The permanent changing of the LES model can lead to an unstable numerical system, as shown in Sagaut (2006). For this reason, the dynamic model is investigated in this work.

- **Wall-Adapting Local Eddy-Viscosity (WALE) Model**

In the WALE model (Nicoud *et al.*, 1999), the eddy viscosity is modeled by:

$$\mu_t = \rho L_s^2 \frac{\left(S_{ij}^d S_{ij}^d\right)^{3/2}}{\left(\bar{S}_{ij}\bar{S}_{ij}\right)^{5/2} + \left(S_{ij}^d S_{ij}^d\right)^{5/4}} \tag{10}$$

Where L_s and S_{ij}^d in the WALE model are defined, respectively, as

$$L_s = \min\left(\kappa d, C_w V^{1/3}\right) \tag{11}$$

$$S_{ij}^d = \frac{1}{2}\left(\bar{g}_{ij}^2 + \bar{g}_{ji}^2\right) - \frac{1}{3}\delta_{ij}\bar{g}_{kk}^2, \quad \bar{g}_{ij} = \frac{\partial \bar{u}_i}{\partial x_j} \tag{12}$$

In ANSYS Fluent, the default value of the WALE constant, C_w is 0.325 and has been found to yield satisfactory results for a wide range of flow. The rest of the notation is the same as for the Smagorinsky-Lilly model.

- **Dynamic Kinetic Energy Subgrid-Scale Model**

The dynamic subgrid-scale kinetic energy model in ANSYS Fluent replicates the model proposed by Kim and Menon (1997). The subgrid-scale kinetic energy is defined as

$$k_{sgs} = \frac{1}{2}\left(\overline{u_k^2} - \bar{u}_k^2\right) \tag{13}$$

The subgrid-scale eddy viscosity, μ_t, is computed using k_{sgs} as

$$\mu_t = C_k\, \rho k_{sgs}^{1/2} \Delta f \tag{14}$$

where Δf is the filter-size computed from $\Delta_f \equiv V^{1/3}$

The subgrid-scale stress can then be written as:

$$\tau_{ij} - \frac{2}{3}\rho k_{sgs}\delta_{ij} = -2C_k\, \rho k_{sgs}^{1/2} \Delta f\ \bar{S}_{ij} \tag{15}$$

k_{sgs} is obtained by solving its transport equation.

$$\rho\frac{\partial \bar{k}_{sgs}}{\partial t} + \rho\frac{\partial \bar{u}_j \bar{k}_{sgs}}{\partial x_j} = -\tau_{ij}\frac{\partial \bar{u}_i}{\partial x_j} - C_\varepsilon \rho\frac{k_{sgs}^{3/2}}{\Delta_f} + \frac{\partial}{\partial x_j}\left(\frac{\mu_t}{\sigma_k}\frac{\partial k_{sgs}}{\partial x_j}\right) \tag{16}$$

Note that the model constants, C_k and C_ε, are determined dynamically (see Kim and Menon 1997). σ_k is hardwired to 1.0. The details of the implementation of this model and its validation can be found in Kim (2004).

4.3. Boundary Conditions (BCs)

Figure 10 presents the BCs of this study. Note that the dimensions of the experimental room are very large comparing to the jet diffusion zone.

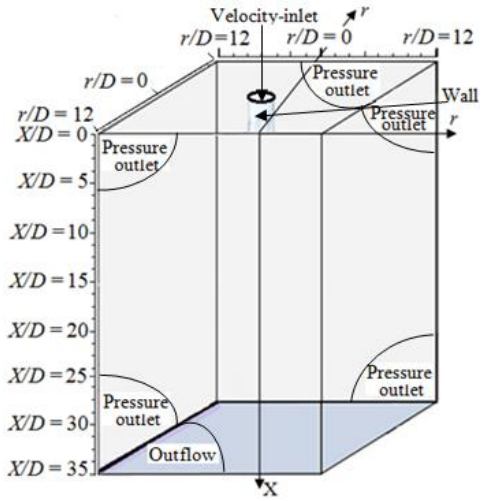

Fig. 10. Computational domain with Boundary conditions.

The BCs for the models of turbulence LES/S-L, LES/WALE and the LES/K-ET are shown in Table 2:

Table 2 Boundary conditions

Nozzle Inlet	U= 7.7 m.s^{-1}, Re= 3.0×10^5 and T=323.3K
Turbulence Intensity	5 %
Relaxation Factors	Pressure = 0.3, Density = 0.9, Energy = 0.9, Moment = 0.6, body forces = 0.9, Turbulent kinetic Energy = 0.7, Specific Dissipation Rate = 0.7, Turbulent Viscosity = 0.9.
Convergence Criterion	Energy =10^{-6} , other parameters =10^{-3}
Pressure-Velocity coupling	SIMPLE
Pressure	Standard

5. NUMERICAL RESULTS AND DISCUSSION

5.1 The Meshing Effect

For the present tridimensional study, Gambit is used to generate the meshing. For the studied cases,the mesh is optimized and validated by comparison with those obtained experimentally.

The independence of the solution with respect to the mesh is studied for the lobed-jets and the swirling jet. The result obtained is illustrated in Figs. 12 to 14.

Figures 12 to 14 show that the radial and axial temperature profiles simulated with the mesh 3 properly reproduce the experimental values. Thereby, the mesh 3 is then picked out to perform the simulations.

5.2 Reduced Axial Temperature Evolution for the Six- Lobed Jet

Figure 15 shows a comparison between the numerical and experimental results relating to the reduced temperature (T_r) in different axial positions. The numerical results are obtained by means of the three turbulence models: LES/SL, LES/WALE and the LES/K-ET.

As it is visible from Fig. 15, in the region near the blowing orifice (potential core region), a good agreement has been obtained between the predicted temperatures with the three turbulence models and the experimental results. There is only the LES/K-ET model which starts to diverge from the axial distance x/D_e=5 (region where the flow is fully developed). The axial temperature predicted with the three turbulence models, LES/S-L, LES/WALE and LES/K-ET, are in good concord with the results of experimental for the prediction of the mean flow close the blow hole. The flow interaction with the diffuser was treating correctly by these models. Similar evolutions of the thermal quantities are unsatisfactory predicted by the LES/S-L turbulence model. In the axial direction, the average error between the results obtained with the LES/S-L, LES/WALE and the LES/K-ET models and the experimental results is 9.60%, 5.47% and 6.69% respectively. Therefore, the predicted temperatures with the LES/WALE model are properly validated.

5.3 Reduced Radial Temperature of the Six- Lobed Jet in the Major and Minor Planes

Reduced radial temperature profiles are shown in Fig. 16 and compared to experimental values at x/D_e = 1, 3, 7 and 15 in the major and minor planes.

For x/D_e=1 to 15 the radial temperatures predicted with the LES/WALE and LES/S-L turbulence models are well validated with the experimental results, contrary to the LES/K-ET models. It is to note that the LES/WALE model is the most performed for both the major and minor planes. In the total domain, the axial temperature evolution (T_r) fails to predict at the same time by all models of turbulence. In the radial directions, the average error between the results obtained with the LES/S-L, LES/WALE and the LES/K-ET models and the experimental results is respectively 6.06%, 4.1% and 5.32%. From the foregoing, it can be stated that it is the LES/WALE model that better reproduces radial and axial jet evolutions (see Fig. 16).

5.4 Reduced Axial Temperature Evolution for the Five-Lobed JET

Figure 17 compares the axial evolution of T_r at different positions.

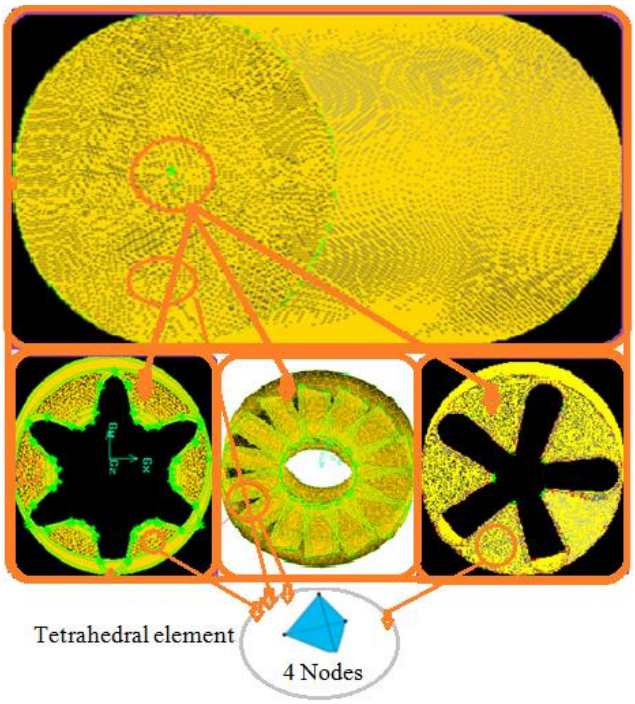

Fig. 11. Computational domain's meshing.

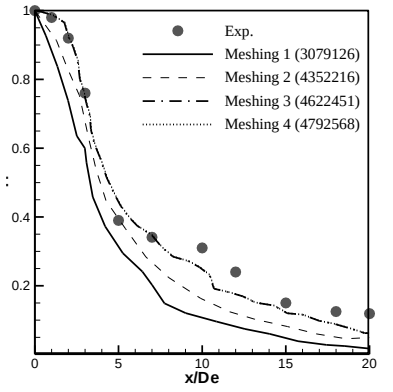

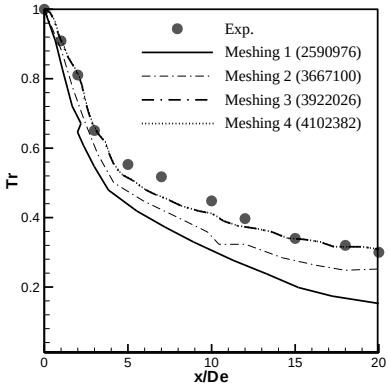

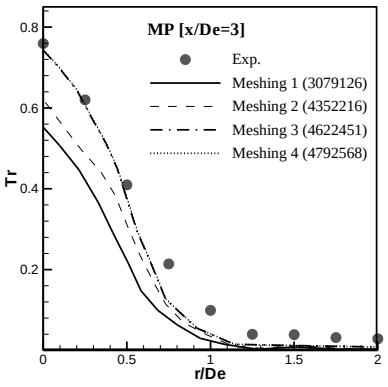

Fig. 12. Independence of the mesh solution for the axial and radial temperature with the LES/WALE (nozzle with 6 lobes).

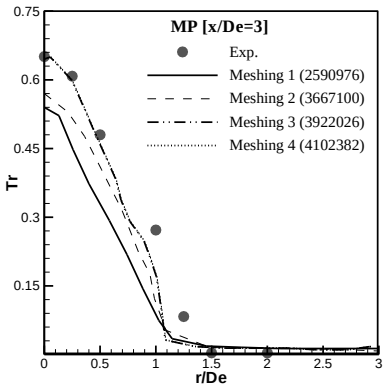

Fig. 13. Independence of the mesh solution for the axial and radial temperature with the LES/WALE (nozzle with 5 lobes).

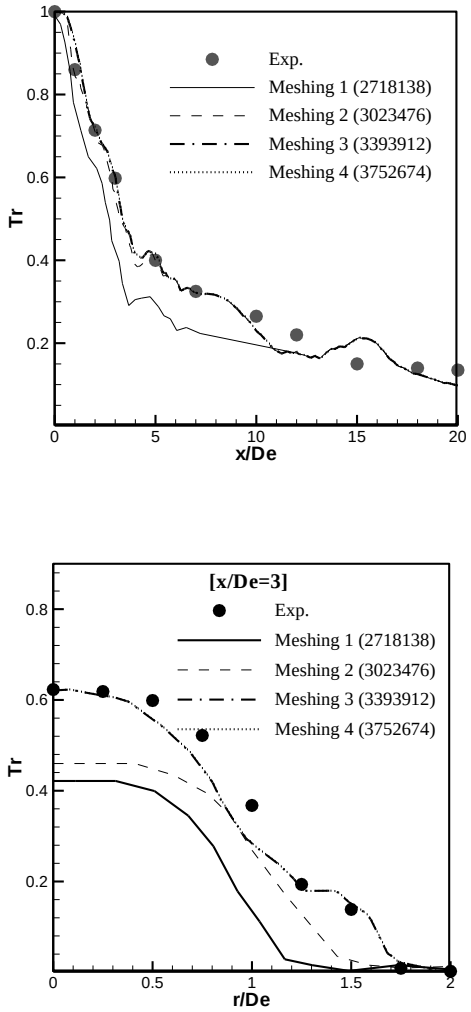

Fig. 14. Independence of the mesh solution for the axial and radial temperature by the LES/K-ET model; case of the swirling nozzle with a tilt angle of 60°.

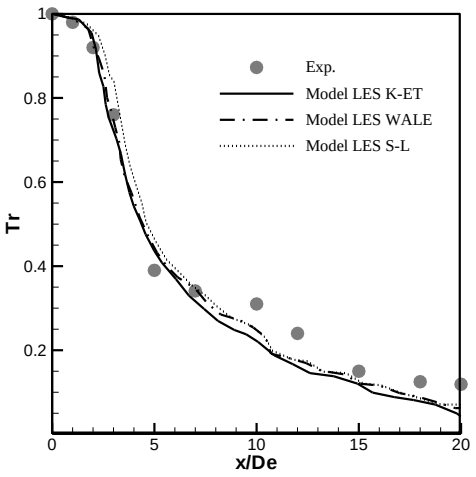

Fig. 15. Comparison of the experimental and numerical temperature axial profile (nozzle with 6 lobes).

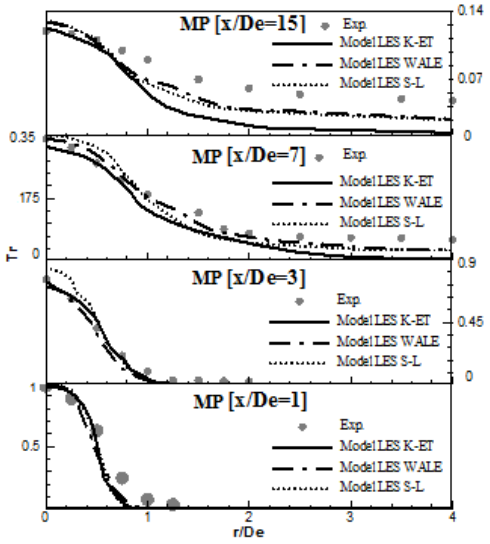

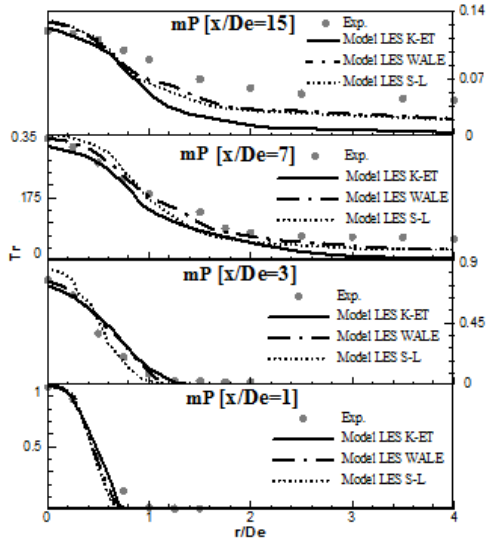

Fig. 16. Comparison of the experimental and numerical radial temperature profiles (MP: Major plane and mP: Minor plane).

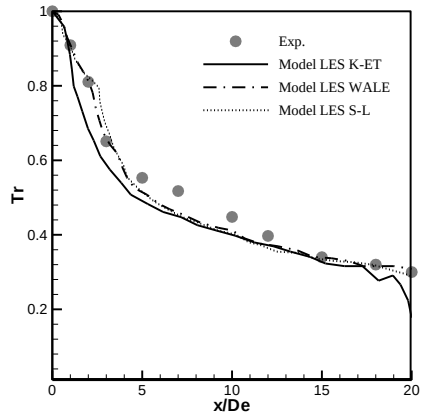

Fig. 17. Comparison of the experimental and numerical temperature in the axial direction (nozzle with 5 lobes).

As can be seen, the LES / WALE and LES / S-L models corroborate the experimental results in the potential core region (close to the blow orifice) with slight differences. Only the LES/K-ET model exhibits deviations from $x/D_e > 1$. The potential core length given by the LES/WALE model is close to that obtained experimentally. In the axial direction, the average error between the results obtained with the LES/S-L, LES/WALE and the LES/K-ET models and the experimental results is 4.42%, 4.07% and 7.13%, respectively. As a result, the LES/WALE model adequately validates the axial temperature profile.

5.5 Reduced Radial Temperature Profiles in the Major and Minor Planes for the Five -Lobed Jet

Figure 18 shows the radial temperature profiles, for the major and minor planes. The three profiles predicted by the LES/S-L, LES/WALE and LES/K-ET models of turbulence are compared to the results of experimental for the different stations (x/D_e=1, 2, 3, 10, 12, and 15). The average error between the results obtained with the LES/S-L, LES/WALE and the LES/K-ET models and the experimental results is respectively 6.90%, 4.42% and 6.13%. The radial temperature profiles predicted by the LES/K-ET model of turbulence depart from the experimental results. However, it turns out that it is the LES/WALE turbulence model that better reproduces the experimental results for both the major and minor planes.

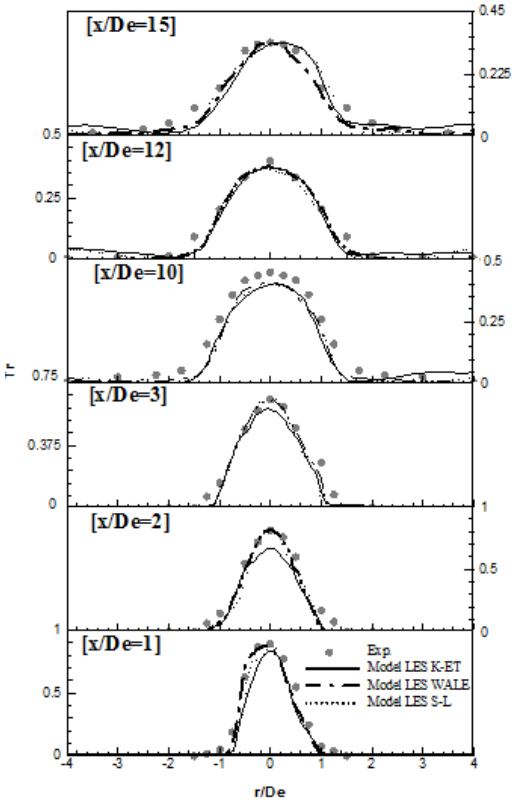

Fig. 18. Comparison of the experimental and numerical radial temperature profiles (Major plane (-) and Minor plane (+)).

5.6 Reduced Axial Temperature Profile for the Swirling Jet

Figure 19 shows the predicted and measured axial temperature profile at different positions.

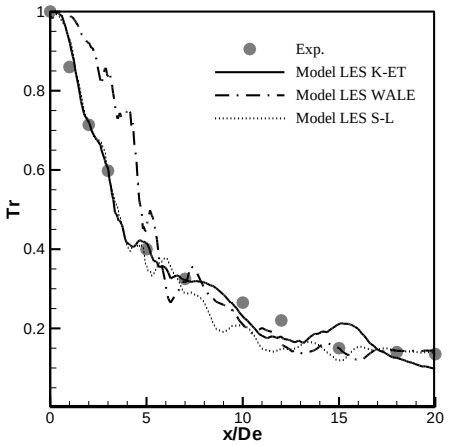

Fig. 19. Comparison of the experimental and numerical axial temperature (swirling jet).

In the total domain, the axial temperature evolution *(T_r)* fail to predict by all models of turbulence at the same time. Figure 19 indicates that the temperatures predicted by the LES/K-ET and LES/S-L turbulence models, in general, are in accordance with the experiment. Starting from the position x/D_e=0 to x/D_e=5, the model LES/WALE gives a similar form with some divergence with the results of experimental. The average error between the results obtained with the LES/S-L, LES/WALE and the LES/K-ET models and the experimental results is 9.28%, 9.56% and 7.58%, respectively. Thus, it is the LES / K-ET turbulence model that correctly validates the axial temperature profile.

5.7 Reduced Radial Temperature Profiles of the Swirling Jet

Figure 20 compares the experimental and numerical radial temperature profiles at x/D_e=3, 5, 7 and 10.

The model of turbulence LES/WALE gives a similar form with some divergence with the results of experimental. The LES/S-L turbulence model, predicts unsatisfying similar evolution of the thermal. Again, in the total domain, all the models of turbulence fail to predict at the same time the radial temperature evolution. The average error between the results obtained with the LES/S-L, LES/WALE and the LES/K-ET models and the experimental results is respectively 6.99%, 11.43% and 5.36%. Such a result shows that the temperatures predicted with the LES / K-ET turbulence model are correctly validated.

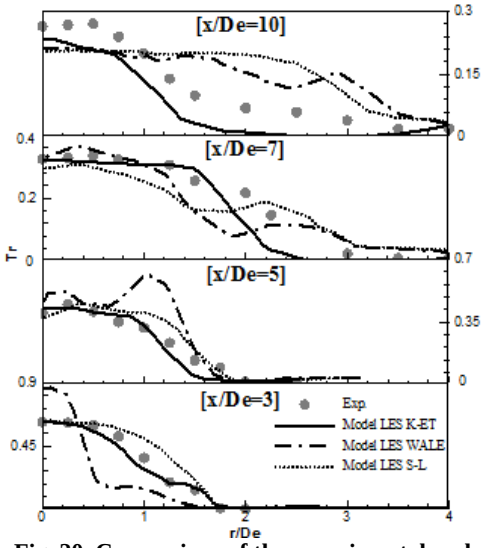

Fig. 20. Comparison of the experimental and numerical radial temperature profiles (swirling jet).

Table 3 Root mean square error (RMSE) between experiment data and model results.

	RMSE		
Turbulence models	LES/WALE	LES/S-L	LES/K-ET
Jet with 5 lobes	0.0424	0.0566	0.0663
Jet with 6 lobes	0.0478	0.0783	0.0600
Swirling jet	0.1063	0.0939	0.0710

The root mean square error (RMSE) being widely used, it has been adopted here to assess the estimate quality. It is defined as follows:

$$\mathbf{RMSE} = \sum \left(\frac{\left(T_{r_{exp}} - T_{r_{nu}} \right)^2}{N} \right)^{\frac{1}{2}} \qquad (17)$$

5.8 Thermal Study of the Initial and Intermediate Region of the Three Jets

5.8.1 Deformation and Thermal Expansion

Figures 21 and 22 show the temperature field obtained by the LES/WALE model for lobed jets and by the LES/K-ET model for the swirling jet, respectively. The isocontours are exhibited in different transverse planes from x/D_e=0.25 up x/D_e=8.0 (see Fig. 21).

From these figures, it can be seen that the signature of the lobes is very marked at x/D_e=0.25 for the lobed jet, and tends to disappear at x/D_e=5 for the 5-lobed jet (Fig.21 (A)) and at x/D_e=3 in for the 6-lobed jet (Fig. 21 (B)). Beyond x/D_e=5, the 6-lobed jet is not influenced by lobes or troughs. The jet behaves like a circular jet while exhibiting similar experimental temperatures and having the same expansion in the radial direction for both the major and minor planes (see Fig. 7).

Note that, beyond $7D_e$ and $8D_e$, the lobes or the troughs do not influence the 5-lobe jet or the swirling jet, respectively. Furthermore, it has been found that the thermal expansion of the 6-lobed jet is greater than that of the 5-lobed jet. it turns out that as the number of lobes increases, the similarity of the profiles is reached more quickly confirming the effectiveness of the 6-lobed jet. In addition, according to their mixing capabilities, the 6-lobed jet is a particularly suitable, followed by the 5-lobed jet and the swirling jet. This finding is corroborated by the experimental results at different radial and axial stations.

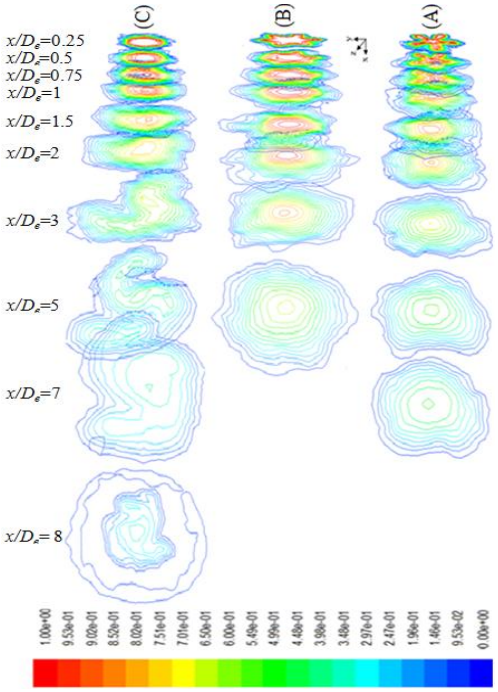

Fig. 21. Temperature contours at different streamwise positions of (A) the 5-lobed nozzle (A); (B) the 6-lobed nozzle and (C) swirling nozzle.

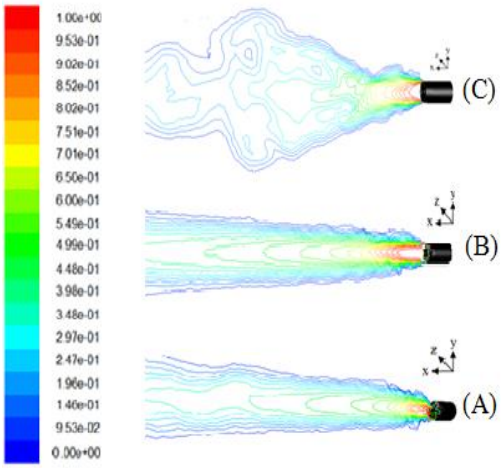

Fig. 22. Streamwise temperature contours; (A) the 5-lobed nozzle, (B) the 6-lobed nozzle with and (C) swirling nozzle.

According to these figures, it was noted that the temperatures are not homogeneous near the blowing orifice but they start to homogenize after a certain radial and axial distance. It has also been found that the swirling jet provides a better radial expansion of temperatures compared to lobed jets. Thereby, the swirling jet seems better suited in the case of large volumes. As for lobed jets, they better ensure the stability of radial temperatures. They are the seat of a large transverse shear due to the inclination of the trough. To sum up, according to the experimental and numerical results of the 6-lobed jet, the homogenization of radial temperatures has been observed at a short distance from the jet axis. However, when the axial distance exceeds x/D_e=5, the temperature begins to homogenize along the flow.

6. CONCLUSION

This work deals with experiments and large-eddy simulations of lobed and swirling turbulent thermal jets for HVAC applications. The aim is to optimize the distribution of air and the thermal field. Such an optimization is achieved on the basis of the thermal prediction (experimental and numerical) of three jets, two being lobed and the third being a swirling jet. Depending on the results obtained, the following conclusions can be drawn:

- Axial temperature profiles have highlighted the importance and role of troughs, number, height and opening of the lobes in the jets mixing performance.
- In the potential core, the thermal profiles are more expansive in the major plane due to the more flared lobes opening.
- In intermediate and fully developed regions, these profiles are not influenced by lobes or troughs. Thereby, the jet is similar to a circular jet allowing for a performance mixture of the lobed jet away from its source.
- The swirling jet with a tilt angle of 60 ° ensures a better expansion of the radial temperature compared to the lobed jet. This asset would be more appropriate for large volumes although lobed jets supply a better stability of radial temperatures.
- The six-lobed nozzle with an opening flared and low height is more effective than others. It provides a good mix and a marked atmosphere homogenization. This corroborates the mixing performance of the 6-lobed jet.
- For lobed jets, it appears that the temperature profiles predicted by the LES/WALE model better corroborate the experimental results than those by the LES/S-L and LES/K-ET models. On the other hand, for the swirling jet, it seems that the temperature profiles predicted by the LES/K-ET model are in good agreement with the experimental results compared to the other models considered here. Therefore, one and the same turbulence model cannot predict simultaneously the whole thermal characteristics of all jets. Moreover, these models cannot simultaneously predict the complete thermal characteristics, in the axial and radial directions. The obtained results show the interest of the characteristics of this type of jet for its application to the residential heating and air conditioning.

REFERENCES

Belovich, V. M. and M. Samimy (1997). Mixing processes in a coaxial geometry with a central lobed mixer-nozzle. *AIAA J* 35(5), 838-841.

Bennia, A., L. Loukarfi, A. Khelil, S. Mohamadi, M. Braikia and H Naji (2018). Experimental and numerical investigation of a turbulent lobed diffuser jet: Application to residential comfort. *Mechanics & Industry*19, 104-115.

Bennia, A., L. Loukarfi, A. Khelil, S. Mohamadi, M. Braikia and H. Naji (2016). Contribution to the Experimental and Numerical Dynamic Study of a Turbulent Jet Issued from Lobed Diffuser. *Journal of Applied Fluid Mechanics* 9(6), 2957-2967.

Bennia, A., L. Loukarfi, M. Braikia, A. Khelil and H. Naji (2015). Experimental study of a jet turbulent diffuser with lobes: Application to comfort in the premises to residential use *Nature & Revue Technology A- Basic Sciences and Engineering 13,* 54-58.

Braikia, M., L. Loukarfi, A. Khelil and H. Naji (2012). Improvement of thermal homogenization using multiple swirling jets. *Thermal Science* 16(1), 239-250.

Choi, S. K. and S. O Kim (2012). Turbulence modeling of natural convection in enclosures: A review. *Journal of Mechanical Science and Technology* 26(1), 283-297.

Clark, R.; J. Ferziger and W. *Reynolds* (1979). Evaluation of subgrid-scale models using an accurately simulated turbulent flow. *Journal of Fluid Mechanics* 91(1), 1-16.

Depuru Mohan, N. K. K., R. Prakash and N. R. Panchapakesan (2015). Mixing Augmentation by Multiple Lobed Jets. *American Journal of Fluid Dynamics* 5(2), 55-64.

Dimotakis, P. E. (2000). The mixing transition in turbulent flows. *Journal of Fluid Mechanics*

Elhassan, M. and A. Meslem (2010). Time-resolved stereoscopic particle image velocimetry investigation of the entrainment in the near field of circular and daisy-shaped orifice jets. *Physics of Fluids* 22(3), 035107.

Elhassan, M., A. Meslem and K. Abed-Meraïm (2011). Experimental investigation of the flow in the near-field of a cross-shaped orifice jet. *Physics of Fluids* 23, 16.

Erlebacher,G., M. Y. Hussaini, C. G. Speziale and T. A. Zang (1992). Toward the Large-Eddy

Simulation of Compressible Turbulent Flows. *Journal of Fluid Mechanics* 238, 155-185.

Germano, M., U. Piomelli, P. Moin and W. H. Cabot (1996). *Dynamic Subgrid-Scale Eddy Viscosity Model*. *In Summer Workshop*. Center for Turbulence Research, Stanford, CA.

Glauser, M., L. Ukeiley and D. Wick (1996). Investigation of turbulent flows via pseudo flow visualization, part 2: the lobed mixer flow field. *Experimental Thermal and Fluid Science* 13(2), 167-177.

Hu, H., H. X. Liu and S. S. Wu (1996). Experimental investigation on the aerodynamic performance of the 2D exhaust ejector system. *ASME 96-GT*, 243.

Hu, H., T. Kobayashi, S. Wu and G. Shen (1999). Changes to the vortical and turbulent structure of jet flows due to mechanical tabs, *Proc. Inst. Mech. Eng* 213, Part C, 321–329.

Hu, H., T. Saga, T. Kobayashi and N. Taniguchi (2000). Passive control on jet mixing flows by using vortex generators, In: *Proceeding of 6th Triennial Int. Symp. on Fluid Control, Measurement, and Visualization*, Sherbrooke, Canada.

Hu, H., T. Saga, T. Kobayashi and N. Taniguchi (2001). A study on a lobed jet mixing flow by using stereoscopic particle image velocimetry technique. *Physics of Fluids* 13(11), 3425-3441.

Jones, D. A. and D. B. Clarke (2008). *Simulation of flow past a sphere using the Fluent code*. Maritime Platforms Division, DSTO Defence Science and Technology Organisation, Australia.

Khelil, A., H. Naji, L. Loukarfi and G. Mompean (2009). Prediction of a High Swirled Natural Gas Diffusion Flame Using a PDF Model. *Fuel* 88(2), 374-381.

Kim, S. E. (2004). Large eddy simulation using unstructured meshes and dynamic subgrid-scale turbulencemodels. Technical Report AIAA-2004-2548. *34th Fluid Dynamics Conference and Exhibit American Institute of Aeronautics and Astronautics*.

Kim,W. W., and S. Menon (1997). Application of the localized dynamic subgrid-scale model to turbulent wall bounded flows". Technical Report AIAA-97-0210. *35th Aerospace Sciences Meeting, Reno, NVAmerican Institute of Aeronautics and Astronautics*.

Lee, S. G. (2008). Experimental investigation of mixing-enhanced swirl flows. *Journal of Mechanical Science and Technology* 22(12), 2509-2515.

Leonard, A. (1974). Energy cascade in large-eddy simulations of turbulent fluid flows. *Advances in Geophysics A* 18, 237-248.

Li-wei, D., L You-hong, S Wan-ren, X Su, D. Hong-wei (April 2015). Effect of lobe number on aerothermodynamic performance of lobed S-shaped two-dimensional nozzle. *Journal of Aerospace Power* 30(4), 916-26.

Meslem, A., A. Dia, C. Beghein, M. El Hassan, I. Nastase and P. J., Vialle (2011). A comparison of three turbulence models for the prediction of parallel lobed jets in perforated panel optimization. *Building and Environment* 46 (11), 2203-2219.

Meslem, A., F. Bode, I. Nastase and O. Martin (2012). Optimization of lobed perforated panel diffuser: numerical study of orifice geometry. *Modern Applied Science* 6(12), 59.

Meslem, A., I. Nastase and F. Allard (2010). Passive mixing control for innovative air diffusion terminal devices for buildings. *Building and Environment* 45(12), 2679-2688.

Meslem, A., I. Nastase and K. Abed-Meraim (2008). Experimental investigation of the mixing performance of a lobed jet flow. *Journal of Engineering Physics and Thermophysics* 81(1), 106–111.

Nastase, I. (2007). *Analysis of lobed jets in order to their integration into the Terminal Units of Air diffusion.* PhD thesis in Civil Engineering, University of La Rochelle, France.

Nastase, I. and A. Meslem (2010). Vortex dynamics and mass entrainment in turbulent lobed jets with and without lobe deflection angles. *Experiments in Fluids* 48(4), 693-714.

Nastase, I., A. Meslem, V. Iordach and I. Colda (2011). Lobed grilles for high mixing ventilation - An experimental analysis in a full scale model room. *Building and Environment* 46, 547-555.

Nicoud, F. and F. Ducros (1999). Subgrid-Scale Stress Modelling Based on the Square of the Velocity Gradient Tensor. *Flow, Turbulence and Combustion* 62(3), 183-200.

Oyakawa, K., M. Yaga, K. Nasu, I. Senaha, S. Matsuda and T. Azama (1998). Impingement heat transfer by jet issuing from a cross-shaped nozzle. *Heat Transfer Japanese Research* 27(3), 192-204.

Palsson, H., F. Beaubert and S. Lalot (2013). Inducing Swirling Flow in Heat Exchanger Pipes for Reduced Fouling Rate. *Heat Transfer Engineering* 34(8), 761-768.

Paterson, R. W. (1982). Turbofan forced mixer nozzle internal flow field NASA CR-3492.

Power, G. D., M. D. McClure and D. Vinh (1994). Advanced IR suppresser design using a combined CFD/test approach. *AIAA* 3215.

Presz, W. M., G. Renyolds and D. McCormick (1994). Thrust augmentation using mixer-ejector-diffuser systems. *AIAA* 0020.

Ranga Dinesh, K. K. J., Jenkins, K. W., Savill, A. M. and Kirkpatrick, M. P (2010). Influence of Bluff-Body and Swirl on Mixing and Intermittency of Jets. *Engineering Applications of Computational Fluid Mechanics* 4(3), 374-386.

Sagaut, P. (2006). *Large Eddy Simulation for Incompressible Flows*. Springer.

Smagorinsky, J (1963). General *Circulation Experiments with the Primitive Equations. I. The Basic Experiment*. *Monthly Weather Review*91, 99-164.

Smith, L. L., A. J. Majamak, I. T. Lam, O. Delabroy, A. R. Karagozian, F. E. Marble and O. I. Smith (1997). Mixing enhancement in a lobed injector. *Physics of Fluids* 9(3), 667-678.

Tilman, T. G. and W. M. Presz (1993). Thrust characteristics of a supersonic mixer ejector. *AIAA* 93, 4345-4352.

Ukeiley, L., M. Glauser, D. Wick (1993). Downstream evolution of POD eigenfunctions in a lobed mixer. *AIAA* 4345.

Ukeley, L., M. Varghese, M. Glauser and D. Valentine (1992). Multifractal analysis of a lobed mixer flowfield utilizing the proper orthogonal decomposition. *AIAA Journal* 30(5), 1260-1267.

Yuan, Y. (2000). *Jet fluid mixing control through manipulation of inviscid flow structures*, Ph. D. Thesis, Virginia Polytechnic Institute and State University.

Zaman, K. B. M. Q. (1996a). Axis switching and spreading of an asymmetric jet: the role of coherent structure dynamics. *Fluid Mechanics*, 316**,** 1-27.

Zaman, K. B. M. Q. (1996b). Spreading characteristics and thrust of jets from asymmetric nozzles. *AIAA Paper*, 96-0200.

Zaman, K. B. M. Q., F. Y. Wang and N. J. Georgiadis (2003). Noise turbulence and thrust of subsonic free jets from lobed nozzles. *AIAA Journal* 41(3), 397-407.